Classical Control System Design and Experiment for the Mini-Mast Truss Structure

Bong Wie*
Arizona State University, Tempe, Arizona 85287
and
Lucas Horta† and Jeff Sulla†
NASA Langley Research Center, Hampton, Virginia 23665

This paper describes control system design and experimental test results for the Mini-Mast truss structure located at the NASA Langley Research Center. Simple classical controllers and their ground test results are presented as a benchmark design for the Mini-Mast. The concepts of non-minimum-phase compensation and periodic disturbance rejection control are experimentally validated. The practicality of a sensor decoupling approach for the classical single-input and single-output control design is also demonstrated. The test results that clearly indicate the undesirable effect of phase lag caused by computational delay and prefiltering are discussed.

Introduction

THE objective of this paper is to describe control system design and the results of active control experiment performed for the Mini-Mast truss structure located at the NASA Langley Research Center, under the NASA Control Structure Interaction (CSI) Guest Investigator Program. The paper provides an overview of the Mini-Mast system, modeling for control design, control synthesis, and closed-loop test results. Simple classical controllers and their ground test results are presented as a benchmark design for the Mini-Mast. In particular, the simplicity and practicality of a classical control approach to the active structural control design are emphasized. Consequently, the theoretical aspects of large space structure control problems are not elaborated in this paper.

The Mini-Mast system[1] consists primarily of a 20-m-long truss beam structure, which is deployed vertically inside a high bay tower, cantilevered from its base on a rigid ground foundation. It represents future deployable trusses to be used in space. The overall system configuration and the actuator /sensor locations are illustrated in Fig. 1. Since this beam structure with significant tip mass is cantilevered to the ground, the overall transient responses are dominated by the first flexible mode in each axis. The 6-Hz second bending mode is widely separated from the 0.8-Hz first bending mode and has a modal contribution one order of magnitude less than the first mode. Following the second bending modes, there are a cluster of local modes and additional global bending, torsion, and axial modes up to 100 Hz.

Consequently, the Mini-Mast represents a typical control-structure interaction problem, where controlling the primary modes always requires consideration of the control interactions with the secondary modes. Even for a collocated actuator and sensor pair, special consideration must be given to the effect of the actuator and sensor dynamics and the phase lag caused by computational delay and prefiltering. In the preliminary control design, the first and second modes in each axis (except the second torsion mode) are considered as the primary modes to be actively damped. The third and higher modes in each axis are considered as the secondary modes, which are not to be destabilized by the primary-mode controller.

The overall goals of Mini-Mast experiments described in this paper are 1) a rapid transient control of the tip deflection to an impulsive disturbance, and 2) a steady-state vibration suppression to periodic disturbances. Control design and test results are presented for two different generic cases: 1) a collocated control using the tip-mounted actuator and sensor pairs, and 2) a noncollocated control using the tip-mounted actuators and noncollocated sensors.

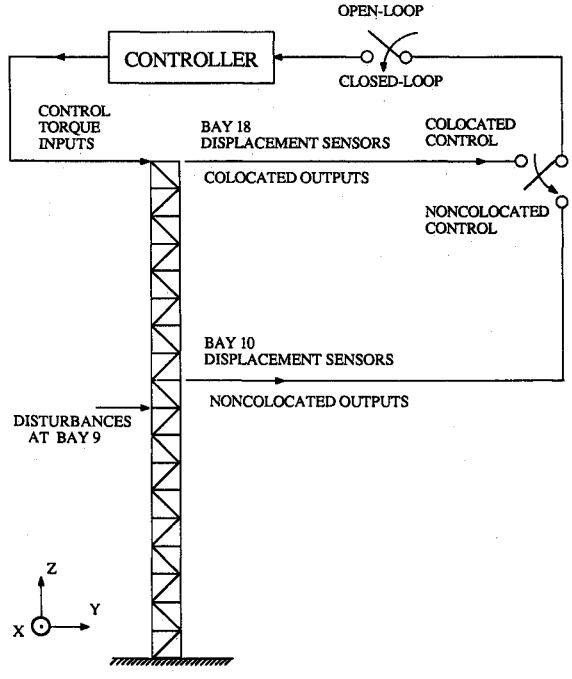

Fig. 1 Schematic representation of Mini-Mast control experiments.

Received March 16, 1990; revision received Sept. 20, 1990; accepted for publication Sept. 23, 1990.

*Associate Professor, Department of Mechanical and Aerospace Engineering. Associate Fellow AIAA.
†Aerospace Engineer, Spacecraft Dynamics Branch, Mail Stop 230. Member AIAA.

Mini-Mast System Description

In this section, the Mini-Mast system is briefly overviewed for the purposes of control design. As illustrated in Fig. 1, the basic element of the system is a 20-m-long, triangular-cross-sectioned, joint-dominated truss structure. An approximately 160-kg tip mass includes three torque wheel actuators (TWAs) mounted on a tip plate at bay 18; the total mass of the system is about 300 kg. A tensioned vertical cable serves to off-load the weight of the tip platform in order to prolong the fatigue life of the system; however, its effect on control experiments should be negligible.

The three TWAs generate orthogonal control torques along the global X, Y, and Z axes. The origin of the global control axes is located at the base of the truss and at the centroid of the triangular cross section, as illustrated in Fig. 2. For disturbance input to the structure, three shakers at bay 9 can be utilized. These shakers are oriented normal to the faces of the truss at each of the three vertices. Displacement sensors used for control experiments are located on the platforms at the tip (bay 18) and near the mid-point of the truss (bay 10). These sensors are positioned to measure deflections normal to the face of the sensor, which are mounted parallel to the flat face on the corner joints on the truss, as shown in Fig. 2. Since the sensor axes are not aligned with the torque wheel axes (i.e., the global X, Y, and Z axes), a coordinate transformation of the sensor outputs is needed for the classical decoupled control design. Such a coordinate transformation or sensor output decoupling matrix is given in Fig. 2.

Experimental, open-loop responses of the Mini-Mast excited by shaker A with a pulse of 100-ms duration and 50-N magnitude are shown in Fig. 3 for the displacement sensor outputs (A, B, and C) and in Fig. 4 for the decoupled outputs (X, Y, and θ). It is evident from Fig. 3 that the overall transient responses at the tip are dominated by the first flexible mode in each axis. The 6-Hz second bending mode, which can be seen at bay 10 responses, is widely separated from the 0.8-Hz first bending mode, and has a modal contribution one order of magnitude less than the first mode. Although there are a cluster of local modes and additional global bending, torsion, and axial modes up to 100 Hz, they are not visible in Fig. 3. The unsymmetric behavior of the Mini-Mast truss structure is also evident in this figure. This effect is probably due to the joint nonlinearity of the truss structure. Despite such a joint nonlinearity problem, the decoupled outputs shown in Fig. 4 clearly indicate the effectiveness of the sensor decoupling concept illustrated in Fig. 2.

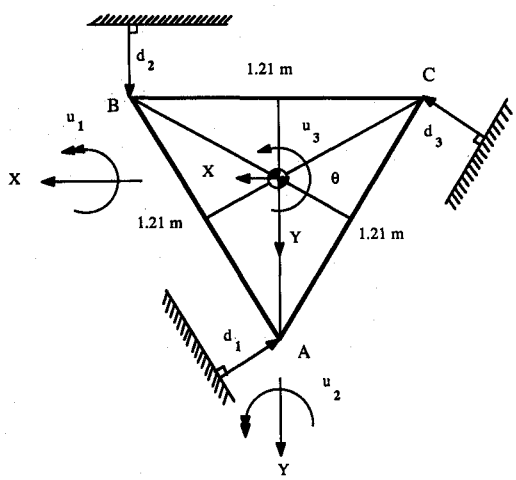

$$\begin{bmatrix} X \\ Y \\ \theta \end{bmatrix} = \begin{bmatrix} -0.57735 & 0 & 0.57735 \\ -0.3333 & 0.6666 & -0.3333 \\ 0.54986 & 0.54986 & 0.54986 \end{bmatrix} \begin{bmatrix} d_1 \\ d_2 \\ d_3 \end{bmatrix}$$

Fig. 2 Schematic diagram of the Mini-Mast cross section and the decoupling matrix.

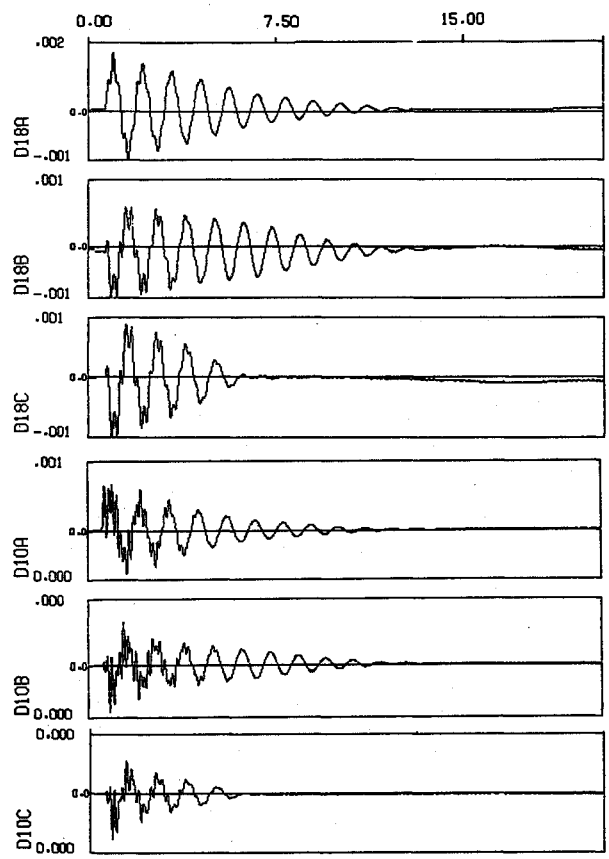

Fig. 3 Open-loop impulse responses for displacement sensors A, B, and C at Bay 10 and Bay 18.

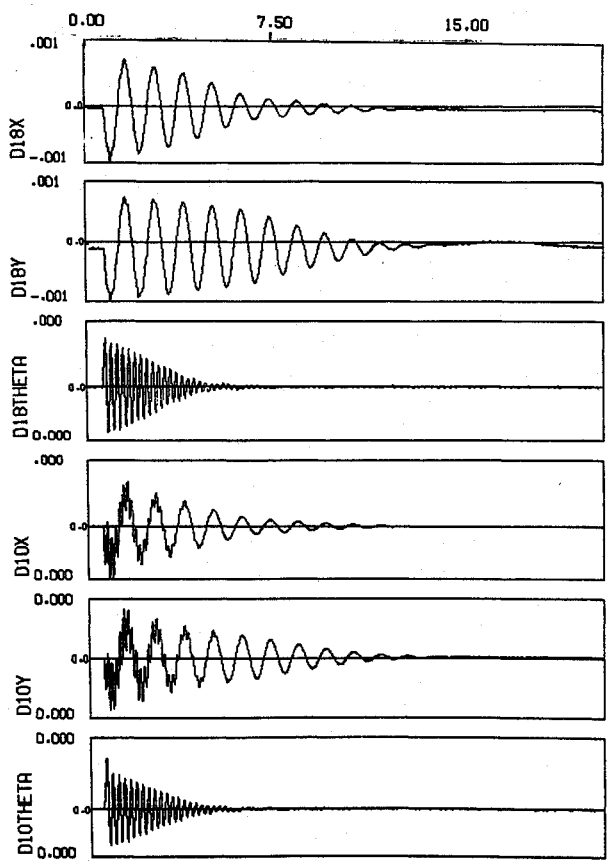

Fig. 4 Open-loop impulse responses for decoupled outputs.

Although there are additional sensors, including accelerometers, distributed along the length of the truss, they are not utilized in the control experiments discussed in this paper.

A simplified transfer function representation of the actuator dynamics used for control design is given as[2]

$$u(s) = \frac{s}{(s/s_1+1)(s/s_2+1)}\, u_c(s) \tag{1}$$

where $u(s)$ is the control torque in units of Nm, $u_c(s)$ the torque wheel angular momemtum command in units of Nms, and s_1 and s_2 the actuator poles. The following numerical values are used for control design: $s_1 = 25\ s^{-1}$ and $s_2 = 300\ s^{-1}$.

Mathematical Modeling for Control Design

A finite element model of the Mini-Mast truss structure developed in Ref. 1 consists of 355 joints and 490 beam elements. Rigid plates are positioned at bays 18 and 10, with appropriate masses for the control hardware. Such a finite element model is represented by

$$M\ddot{q} + Kq = f \tag{2}$$

where M is a positive definite mass matrix, K a positive semidefinite stiffness matrix, q a generalized nodal coordinate vector, and f a vector of external forces and/or torques. Equation (2) is transformed into the following modal equation:

$$\ddot{\eta} + \Omega^2\eta = \Phi^T f \tag{3}$$

where η is a modal coordinate vector, $\Omega = \text{diag}(\omega_i)$, and ω_i is the ith modal frequency. Passive damping is often modeled with a modal damping matrix.

A summary of the modal frequencies and modal damping ratios for the first five modes identified by modal tests is provided in Table 1. Modal damping ratios for the higher frequency modes are assumed to be 1%. There are five modes below 10 Hz. The first two, at approximately 0.8 Hz, are first bending modes oriented nearly in the global X and Y axes. Next is the first torsion mode at 4.4 Hz. It is slightly coupled with bending. The fourth and fifth modes are second bending modes. Unlike the first bending modes, however, the direction of motion for second bending has rotated 45 deg from the global X and Y axes. This phenomenon results in the coupled second bending modes. Following the second bending modes, there are a cluster of 108 local modes. These modes involve mainly the bending of the diagonal truss members. Following this cluster of local modes, there are additional global bending, torsion, and axial modes up to 100 Hz. In the control design, the first five modes are considered as the primary modes to be actively damped. The sixth and higher modes are considered as the secondary modes, which are not to be destabilized by the primary-mode controller.

Control Design Approaches and Objectives

State-space methods for control design of flexible space structures have been emphasized in the literature and more widely explored than classical methods. There has also been a growing research interest in robust H_∞ control and robustness analysis applied to the control problems of flexible space structures and the space station (e.g., see Refs. 3–5). However, the classical control approach[6–8] was employed for Mini-Mast control experiments and the objective was to investigate the fundamental nature of control-structure interaction problems and to further understand the practical effects of many simplifying assumptions on a realistic space truss structure such as the Mini-Mast.

In particular, a new concept of generalized structural filtering for flexible-mode stabilization, proposed in Ref. 8, and a periodic disturbance rejection concept, which are proposed for the Space Station Freedom[9] and further developed in Refs. 10 and 11, were to be validated by Mini-Mast control experiments. The simplicity and practicality of the classical control approach were to be demonstrated for the Mini-Mast. The practicality of a sensor decoupling approach was also to be demonstrated for the inherent multivariable control problem of the Mini-Mast.

Table 1 Mini-Mast modal properties

Mode	Frequency, Hz	Damping ratio, %
1st X bending	0.801	1.964
1st Y bending	0.801	1.964
1st torsion	4.364	1.660
2nd XY bending	6.104	1.194
2nd YX bending	6.156	1.194

The control objectives of Mini-Mast experiments described in this paper are 1) a rapid transient vibration control of the tip deflection to an impulsive disturbance, and 2) a steady-state vibration suppression to periodic disturbances. Control design and tests are performed for two different generic cases: 1) a collocated control using the tip-mounted actuator and sensor pairs at bay 18, and 2) a noncollocated control using the tip-mounted actuators at bay 18 and noncollocated sensors at bay 10. The external disturbances are generated by shakers at bay 9. In fact, there exists a multivariable control issue for both cases, because the sensor axes are not aligned with the control input axes. A sensor decoupling approach is, however, used to simplify the control design, which allows the use of a classical single-input single-output (SISO) control method.

In the next section, such a classical SISO control design approach is briefly reviewed, with special emphasis on the concepts of generalized structural filtering and periodic disturbance rejection.

Classical Control Design

Generalized Structural Filtering Concept

In general, the classical gain/phase stabilization concepts are very useful for designing a SISO compensator. These classical control concepts are now significantly enhanced by the new concept of generalized structural filtering, especially with non-minimum-phase zeros.[8] A generalized second-order filter with arbitrary complex poles and zeros is simply represented as

$$\frac{s^2/\omega_z^2 + 2\zeta_z s/\omega_z + 1}{s^2/\omega_p^2 + 2\zeta_p s/\omega_p + 1} \tag{4}$$

By different choices of the coefficients, several well-known frequency shaping filters can be realized. For $\omega_z = \omega_p$ and $\zeta_z = 0$, we have a notch filter for gain stabilization. The notch sharpness depends on the damping ratio of the notch pole. Great care must be exercised in selecting the parameters of the notch filter because of its phase lag at low frequency and its sensitivity to frequency uncertainty. For $\omega_p > \omega_z$ (and usually $\zeta_p = \zeta_z$), we have a complex phase-lead filter for phase stabilization. The amount of phase lead depends primarily on the ω_p/ω_z ratio, but the ratio should not be too high because of the gain increase at higher frequencies. Without the filter zeros, we have a simple rolloff filter.

The filters just discussed are minimum phase, i.e., the filter poles and zeros are on the left-half s-plane. However, a variety of non-minimum-phase filters ($\zeta < 0$) studied in Ref. 8 have very interesting gain/phase characteristics that are useful for flexible-mode stabilization. The non-minimum-phase filtering, as opposed to the minimum-phase filtering, provides the proper phasing to increase the closed-loop damping ratio of the flexible modes while maintaining a good robustness property to the model uncertainty.[3,4,8]

Because of such a generalized structural filtering concept, the classical direct frequency shaping technique based on the gain/phase stabilization concepts is now significantly enhanced. Consequently, the design of a SISO compensator is

simply carried out starting with the stabilization of the primary mode and subsequent analysis and stabilization of any unstably interacting flexible modes. Feedback control with a noncollocated actuator and sensor pair generally results in the presence of unstably interacting flexible modes. After the unstably interacting modes have been identified, proper filtering to phase or gain stabilize those modes is then introduced. Also, periodic disturbance rejection filtering is synthesized to compensate for any periodic disturbances acting on the structure. Aided by the root locus method and mode plots, and a certain amount of trial and error, a robust compensator design is performed.

Active Disturbance Rejection

Active disturbance rejection control synthesis is simply achieved by introducing into the feedback loop a model of the disturbance.[10-12] It is assumed that a persistent disturbance with one or more frequency components is modeled as

$$w(t) = \sum_i A_i \sin(p_i t + \phi_i) \tag{5}$$

with unknown magnitudes A_i and phases ϕ_i but known frequencies p_i. The disturbance $w(t)$ can be described by a Laplace transformation $w(s) = N_w(s)/D_w(s)$, where $N_w(s)$ is arbitrary as long as $w(s)$ remains proper. The roots of $D_w(s)$ correspond to the frequency components of a periodic disturbance. The inclusion of the disturbance model $1/D_w(s)$ inside the control loop is often referred to as the internal modeling of the disturbance. In classical design, the internal disturbance model is regarded as being part of the compensator, as shown in Fig. 5a.

The presence of $1/D_w(s)$ in the control loop results in the effective cancellation of the poles of $w(s)$, provided that no root of $D_w(s)$ is a zero of the plant transfer function. This is shown in the following equations:

$$y(s) = \frac{1/D(s)}{1 + N_c(s)N(s)/D_c(s)D_w(s)D(s)}\, w(s)$$

$$= \frac{D_c(s)D_w(s)}{D_c(s)D_w(s)D(s) + N_c(s)N(s)} \frac{N_w(s)}{D_w(s)} \tag{6}$$

As illustrated in Fig. 5b, the compensator can be viewed as a series of individual filters. Each filter is designed to perform a specific task, like the stabilization of a particular mode for example. In the same manner, a disturbance rejection filter can be designed. That is, a numerator is properly chosen in the compensator to go together with the disturbance model, as

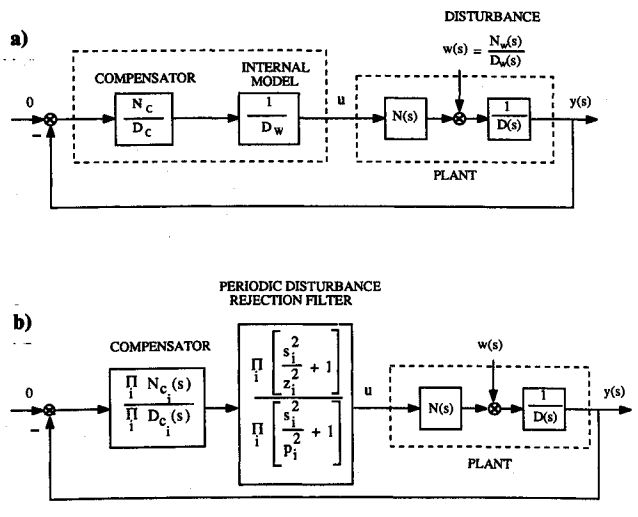

Fig. 5 Block diagram representation of the periodic disturbance rejection controller.

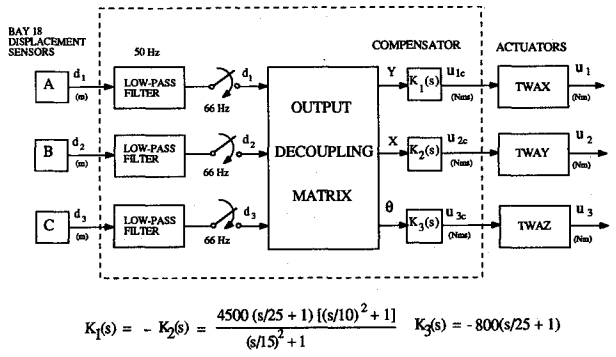

Fig. 6 Collocated controller with periodic disturbance rejection filtering for X and Y at Bay 18.

shown in Fig. 5b. The numerator is chosen to be of the same order as $D_w(s)$ so that there is a zero for each pole of the disturbance model. The presence of the disturbance model directly translates into a control input with components that will effectively cancel the periodic disturbance. Detailed discussions of both classical and state-space methods for periodic disturbance rejection control synthesis can be found in Refs. 9-11.

Although the active disturbance rejection concept based on the internal model principle has been well known (e.g, see Ref. 12), an interesting interpretation of the concept from a classical control viewpoint is given here. Each pole-zero combination of the periodic disturbance rejection filter can be called a dipole. The filter thus consists of as many dipoles as there are frequency components in the periodic disturbance. The separation between the zero and the pole is generally referred to as the strength of the dipole. The strength of the dipole affects the settling time of the compensated system; the larger the separation between the pole and zero of the filter, the shorter the settling time. This is caused by the position of the closed-loop pole corresponding to the disturbance frequency. As the strength of the dipole is increased, this pole is pushed farther to the left, speeding up the response time of the disturbance rejection. However, this separation influences the gain characteristics of the plant because the dipole presents a certain amount of magnitude in the neighborhood of the pole and zero frequencies. Moreover, at frequencies higher than the dipole, there is a net gain increase or reduction. The magnitude of this gain increases with the separation between pole and zero. Therefore, as the strength of the dipole is changed to meet a chosen settling time, the compensation must be readjusted. A compromise has to be reached often between the settling time and the stability of the closed-loop system.[10,11]

Collocated Control Design and Experiments

A simplified control loop block diagram is shown in Fig. 6 for collocated control experiments using the tip-mounted actuators and displacement sensors A, B, and C at bay 18. The sensor outputs are low-pass filtered by an analog, three-pole Bessel filter with a corner frequency of 50-Hz in each axis. (Although a 50-Hz filter was used in the control design, it was found during the final stages of testing that a 20-Hz filter was mistakenly selected. The resulting effect was significant and will be discussed later in this section.) The global X- and Y-axes bending and Z-axis torsional displacements at bay 18 are generated by using the output decoupling matrix given in Fig. 2. The Y/u_1 transfer function has alternating poles and zeros along the imaginary axis. The X/u_2 and θ/u_3 transfer functions also have such a collocated actuator-sensor property. As a result, a SISO collocated control design is possible, where the TWAs at the tip provide the control inputs and the global displacements of the tip (bay 18) are fed back with proportional gains. Thus, direct feedback of the decoupled

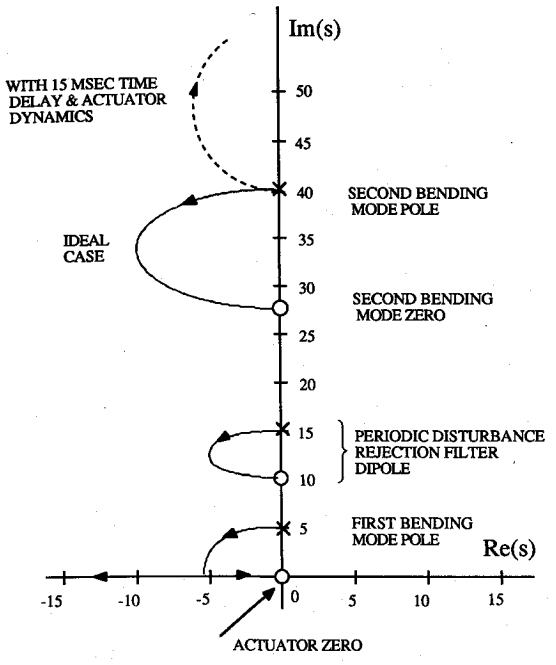

Fig. 7 Root locus vs the overall loop gain of the collocated X-axis controller.

displacement outputs (X, Y, θ) is the basic element of the collocated control experiments for the Mini-Mast using the torque wheel actuators whose dynamics are characterized by Eq. (1). However, a proportional and derivative (PD) control is needed to effectively compensate the actuator dynamics at near its high-pass break frequency. The PD compensator zero is chosen near the actuator pole at $s = -25$. A mismatching of the actuator pole by the PD compensation zero is not significant. An effective control loop delay of 15 ms from digital control implementation with a sampling rate of 66.6 Hz is assumed. Such a time delay causes approximately 33-deg phase lag at the second bending mode frequency of 38 rad/s (6.1 Hz).

To validate the concept of active disturbance rejection for flexible space structures, a case with a sinusoidal disturbance with known frequency of 15 rad/s and unknown magnitude of 5 N is considered. Such a sinusoidal disturbance is generated by shaker A at bay 9, and disturbance rejection for the X- and Y-axes bending at the tip is considered. The compensator for this case, given in Fig. 6, includes a dipole for periodic disturbance rejection with the pole at $s = \pm j15$ and the zero at $s = \pm j10$, so that the zero lies between two consecutive poles of the loop transfer function. Figure 7 shows the locus of closed-loop poles vs the overall loop gain for the X-axis control loop with the periodic disturbance rejection filter dipole.

The first test of this collocated controller was to investigate the closed-loop behavior to an impulsive disturbance. Figure 8 shows the closed-loop tip response of this controller for the same impulse disturbance as for Figs. 3 and 4. A 20% active damping ratio for the first mode in each axis has been achieved, as predicted by design. However, an undesirable phenomenon is evident in Fig. 8; that is, the second bending modes become less stable. This anomaly, which was not predicted by design, was found to be caused probably by the mistakenly selected analog prefilter of 20-Hz (instead of 50-Hz) corner frequency. Additional test results with a 50-Hz filter indicate less destabilization of the second bending modes, but the second bending modes were still gain stabilized. The late discovery of this problem prevented a redesign of the collocated controller.

The test cycle proceeded with the sinusoidal disturbance. It was demonstrated that a periodic disturbance rejection can be achieved for the outputs X and Y at bay 18.[13] In this case, the

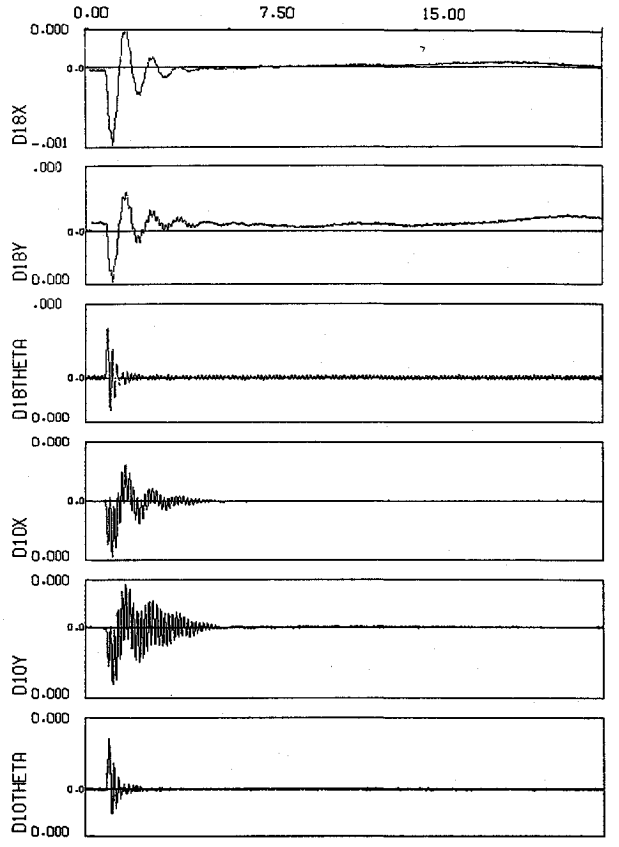

Fig. 8 Closed-loop impulse responses of the collocated controller.

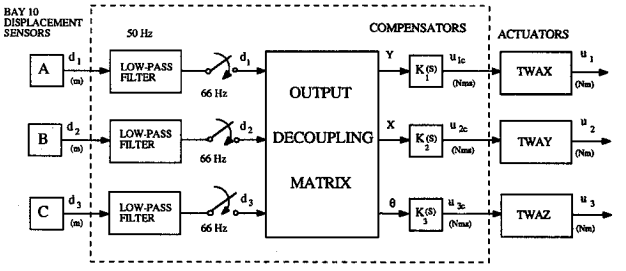

$$K_1(s) = -K_2(s) = \frac{-6000(s/25+1)[(s/20)^2+1][(s/4.9)^2-1.4s/4.9+1]}{[(s/15)^2+1][(s/4.9)^2+1.4s/4.9+1]}$$

$$K_3(s) = -800(s/25+1)$$

Fig. 9 Noncollocated controller with periodic disturbance rejection filtering for X and Y at Bay 10.

control inputs u_1 and u_2 present a steady-state oscillation caused by the dipole, which counteracts the periodic disturbance applied on the system.

Noncollocated Control Design and Experiments

A case of further interest is the case where the controller uses displacement sensors that are not located at the tip but at the midsection (bay 10), resulting in a noncollocated control configuration. Figure 9 shows a control system block diagram for this noncollocated case, with non-minimum-phase compensation and with periodic disturbance rejection filtering for X and Y at bay 10.

Similar to the collocated case, the sensor outputs are low-pass filtered by an analog, three-pole Bessel filter with a corner

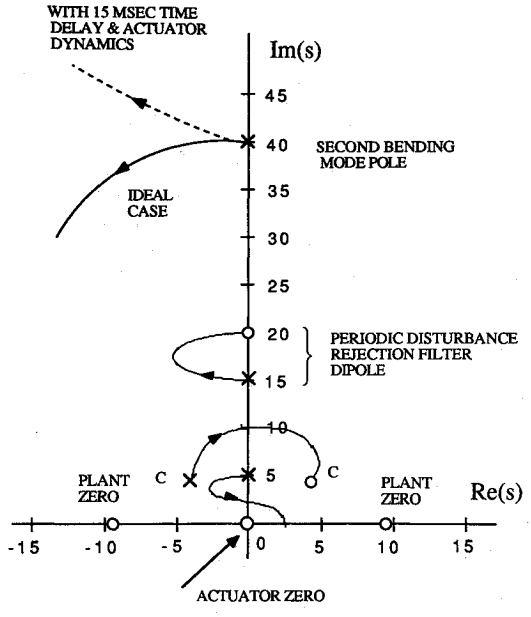

Fig. 10 Root locus vs the overall loop gain of the noncollocated X-axis controller.

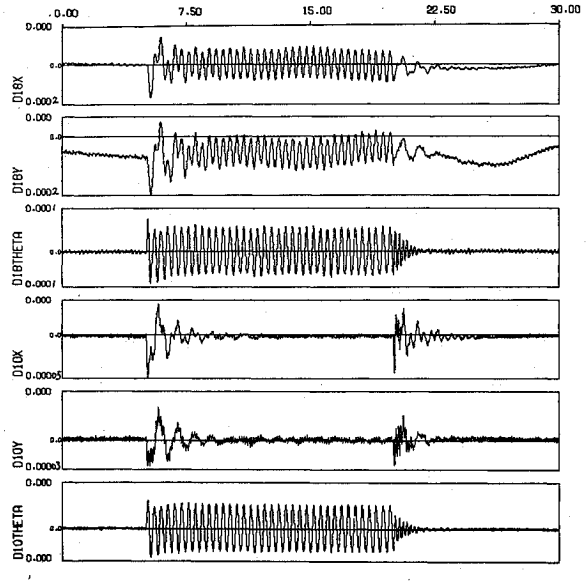

Fig. 11 Closed-loop sinusoidal responses of the noncollocated controller with disturbance rejection for X and Y at Bay 10.

frequency of 50 Hz in each axis. Then, the global X- and Y-axes bending and Z-axis torsional displacements at bay 10 are generated by using the output decoupling matrix. The Y/u_1 transfer function has nonalternating poles and zeros along the imaginary axis. The X/u_2 and θ/u_3 transfer functions also have such a noncollocated actuator-sensor property. A SISO control design, however, is still possible, where the TWAs at the tip provide the control inputs and the global displacements at bay 10 are fed back with proper compensation.

The test results[13] for a case where the Mini-Mast is excited by shaker A with a pulse of 100-ms duration and 50-N magnitude show that the noncollocated control system, shown in Fig. 9, without the disturbance rejection filter dipole, has a 15% damping ratio for the first mode in each axis.

To validate the concept of periodic disturbance rejection for flexible space structures, even for the noncollocated case, a case with a sinusoidal disturbance with known frequency of 15 rad/s and disturbance rejection for the X- and Y-axes bending at bay 10 is considered. The compensator for this case, given in Fig. 9, includes a dipole for periodic disturbance rejection with the pole at $s = \pm j15$. The zero corresponding to the dipole is placed at $s = \pm j20$, between the consecutive poles of the dipole and the second bending mode.

Figure 10 shows the locus of closed-loop poles vs overall loop gain for the X-axis control loop with both non-minimum-phase compensation and the periodic disturbance rejection filter dipole. Test results shown in Fig. 11 demonstrate that a periodic disturbance rejection can be achieved for the outputs X and Y at bay 10. Shaker A is turned on at $t = 5$ s and turned off at $t = 20$ s. The closed-loop system is stable and the control inputs u_1 and u_2 (at bay 18) present a steady-state oscillation caused by the dipole, which counteracts the periodic disturbance applied on the system (at bay 9).

Discussion

In the preliminary control design for the Mini-Mast, the first and second modes in each axis (except the second torsion mode) were considered as the primary modes to be actively damped. The third and higher modes in each axis were considered as the secondary modes that were not to be destabilized by the primary-mode controller. However, during the test cycle, it became clear that active control (i.e., phase stabilization) of the second bending modes was not practical in the presence of significant phase lag caused by the analog prefilter and computational time delay. Consequently, the second bending mode in each axis were gain stabilized, which undoubtedly caused some transient performance degradation at bay 10, as can be seen in Fig. 8. An approach to actively control the second bending modes is to employ a complex phase lead filter[8]; however, test constraints and unmodeled high-frequency dynamics prevented further refinement of the simple classical collocated controller shown in Fig. 6.

In summary, despite the second bending mode anomaly, the concept of non-minimum-phase compensation for the noncollocated control problem and the periodic disturbance rejection filter concept were successfully demonstrated for the Mini-Mast. The effectiveness of the sensor decoupling concept was also successfully validated.

Conclusions

The active structural control design and experimental test results for the Mini-Mast truss structure located at the NASA Langley Research Center have been presented. The simplicity and practicality of a classical control synthesis approach, enhanced by the concepts of non-minimum-phase filtering and active rejection of persistent disturbances, were demonstrated. The test results have shown that the Mini-Mast can be an excellent generic test bed for validating the active vibration control technology for future large space structures. An important lesson learned from the Mini-Mast experiment is that even the single-input and single-output, collocated control design is a nontrivial task in practice.

Acknowledgment

This research was supported by the NASA Langley Research Center under the Control Structure Interaction Guest Investigator Program.

References

[1]Pappa, R. et al., "Mini-Mast CSI Testbed User's Guide," NASA Langley Research Center, Hampton, VA, March 1989.

[2]Taylor, L. W., and Rainy, D. W., "Torque Wheel Actuator Dynamics: Mini-Mast CSI Testbed," NASA Langley Research Center, Hampton, VA, July 1989.

[3]Byun, K.-W., Wie, B., and Sunkel, J., "Robust Control Synthesis for Uncertain Dynamical Systems," AIAA Paper 89-3516, Aug. 1989.

[4]Wedell, E., Chuang, C.-H., and Wie, B., "Stability Robustness Margin Computation for Structured Real-Parameter Perturbations," *Journal of Guidance, Control, and Dynamics,* Vol. 14, No. 3, 1991, pp. 607–614.

[5]Byun, K.-W., Wie, B., Geller, D., and Sunkel, J., "New Robust H_∞ Control Design for the Space Station with Structured Parameter Uncertainty," AIAA Paper 90-3319, Aug. 1990.

[6]Wie, B., and Bryson, A. E., Jr., "Pole-Zero Modeling of Flexible Space Structures," *Journal of Guidance, Control, and Dynamics,* Vol. 11, No. 6, 1988, pp. 554–561.

[7]Wie, B., "Active Vibration Control Synthesis for the COFS-I," *Journal of Guidance, Control, and Dynamics,* Vol. 11, No. 3, 1988, pp. 271–276.

[8]Wie, B., and Byun, K., "New Generalized Structural Filtering Concept for Active Vibration Control Synthesis," *Journal of Guidance, Control, and Dynamics,* Vol. 12, No. 2, 1989, pp. 147–154.

[9]Wie, B., Byun, K. W., Warren, V. W., Geller, D., Long, D., and Sunkel, J., "New Approach to Attitude/Momentum Control for the Space Station," *Journal of Guidance, Control, and Dynamics,* Vol. 12, No. 5, 1989, pp. 714–722.

[10]Wie, B., and Gonzalez, M., "Active Control Synthesis for Flexible Space Structures Excited by Persistent Disturbances," AIAA Paper 90-3427, Aug. 1990.

[11]Wie, B., Liu, Q., and Byun, K.-W., "Robust H_∞ Control Design Method and Its Application to a Benchmark Problem," *Journal of Guidance, Control, and Dynamics* (to be published).

[12]Chen, C. T., *Linear System Theory and Design,* CBS, New York, 1984, pp. 488–506.

[13]Anon., *CSI Phase I Guest Investigator Year-End Review,* Control Structure Interaction Program Office, NASA Langley Research Center, Hampton, VA, Jan. 1990, pp. 97–121.